Microelectronic Engineering 227 (2020) 111314

Contents lists available at ScienceDirect

Microelectronic Engineering

journal homepage: www.elsevier.com/locate/mee

Research paper

Machine learning based technique towards smart laser fabrication of CGH

Aggeliki Anastasiou[a,*], Evangelia I. Zacharaki[b], Dimitris Alexandropoulos[a], Konstantinos Moustakas[b], Nikolaos A. Vainos[a]

[a] Department of Materials Science, University of Patras, Rio, Patra, Greece
[b] Department of Electrical and Computer Engineering, University of Patras, Rio, Patra, Greece

ARTICLE INFO

Keywords:
CGH
Laser materials processing
Regression
Machine learning
Image processing
Gabor features

ABSTRACT

Fabrication of Computer-Generated Holograms (CGHs) on metal surfaces is a challenging procedure, given the nature of the laser-matter interaction specified for metals, and the power requirements for silver laser machining. A machine learning approach is derived for engraving of CGHs on silver surfaces with a 1070 nm fiber laser. The proposed method paves the way towards an automated solution for the fabrication of CGH on silver surfaces that accounts for, in terms of manufacturability. Sophisticated image-based descriptors are extracted from digital holographic masks produced by commercial CGH design software to predict, using machine learning, a "quality score" from '1' to '5', estimating the fabrication feasibility of a CGH's mask. Based on this idea, the procedure of CGH engraving on silver is remarkably improved.

1. Introduction

Computer-generated holograms (CGHs) are diffractive optical elements that have been widely used in a range of domains and applications from microscopy and 3D imaging of biological specimens [1,2], to multiple 3D image encryption [3,4]. The ability to generate objects in different types of display, that do not realistically exist, and then obtain their reconstructed projection reveals various potentials but also generates numerous limitations [5]. Although digital holography has been upgraded thanks to sophisticated techniques and algorithms, that can simulate wavefront propagation phenomena [6,7] and fast computing, there are still difficulties either on engraving procedures and reconstruction of photo-realistic 3D images [6]. Regarding the engravings in metals, there are various applications mainly on security issues (watermarks, QR and DM codes), where fabrication of CGHs is vital to prevent replication of the structures that protect encoding information [8].

Published research works, which were focused on optimization techniques in this field, target mainly the reduction of computational time or memory requirements and provide suggestions concerning the efficiency in calculation and projection of the reconstructed image of a hologram [9]. Chen et al. [10] used point cloud representation combined with a Gaussian interpolation algorithm adjusted to data-parallel computing on graphic processed units to simplify and accelerate occlusion computation, providing a realistic reconstruction. On the same path, Wakunami et al. [6] proposed an optimized calculation of the occlusion culling based on the conversion between light-rays and wavefront with high accuracy on the reproduction of a deep 3D scene. Tsang et al. [11] presented a method for fast numerical generation and encryption of a Fresnel hologram with small number of computations. Encryption accomplished by applying convolution on the reference signal with a key function in the form of a maximum length sequence, also known as M-sequence. The work of Hasegawa et al. [12] describes an optimization process for CGH engraving with femtosecond laser based on a method called second-harmonic optimization. The automatic estimation of pulse peak intensity, which is related to pulse width and spatial pulse profile proved to be an efficient technique. Finally, Pan et al. [13] implemented an alternative polygon-based method to compute a hologram. Starting from a primitive polygon and using matrix pseudo-inversion, interpolation and computation of the power spectral density, the proposed algorithm presents a fast solution with a remarkable quality, concerning the reconstructed image.

The construction of robust and "hard-to-replicate" markings on security applications has a great impact on authentication and quality assurance of products and services. In early studies, several attempts were made to create black and color markings on stainless steel with fiber lasers [14–16]. Their reliability depends more on the exclusive engraving protocol and the adequate parameter selection needed to reproduce them. Martinez et al. [17,18] were the first that presented aesthetic holographic watermarks, based on complementary holography of Lohmann type CGH (detour phase hologram) [19]. Their work demonstrates two versions of watermarking, in binary and grey-

* Corresponding author.
E-mail address: anastasiou@ece.upatras.gr (A. Anastasiou).

https://doi.org/10.1016/j.mee.2020.111314
Received 18 November 2019; Received in revised form 8 March 2020; Accepted 6 April 2020
Available online 09 April 2020

tone image, over phase transition material (PTM) with laser lithography. Engraving of aesthetic holographic structures and microstructures on metal surfaces for anti-counterfeiting applications were initiated by Wlodarczyk et al. [20] for non-detour phase holograms this time. Liquid–crystal-based spatial light modulator (LC-SLM) were used for laser marking processes with picosecond laser. Then, on an optimized version, using a 35 ns UV pulsed laser, new tamper-proof phase holographic microstructures were created on stainless steel with a procedure that provides a localised laser melting process [21]. Similar approaches concerned multi-level phase holograms on glass substrates [22], nickel and Inconel alloys [23]. An increased robustness factor was also introduced in [8], where CGH microstructures were combined with patterns of easy to read messages on a range of conventional markings (QR code, Data Matrices codes, method known as Steganography. Structures that were created on stainless steel with UV nanosecond pulsed laser provided a quality multi-phase level hologram with a suppress twin image and resulted to QR codes with embedded additional securing features.

All the aforementioned work considered, describes mostly procedures for watermarks and engravings on stainless steel, nickel and alloys using lasers CO_2 or UV nanosecond lasers. Hence the range CGHs that can be fabricated using low cost nanosecond laser sources is limited. In this paper, the objective is the construction of CGHs on silver surfaces exploiting the low-cost and industrial technology of a fiber laser. Fiber lasers combine the benefits of an energy-efficient and long-life solution that provides a simpler, smaller, and more reliable system to any industry using automated procedures to build manufacturing lines [24,25].

Silver is one of the most reflective materials, as it can reflect around 95% of visible light, and remains a challenging material for CGH micromachining, even for a fiber laser. In order to facilitate the fabrication of CGHs on metals using laser engraving, in the present work we developed a novel approach that combines image processing and machine learning techniques for the optimization of the design of CGHs in terms of their manufacturability. In the following section, we first presented details on the software used for the creation of the holographic masks and the procedure followed for the assignment of a quality-engraving score and, then we described the dataset and the machine learning method used for training of our prediction model. Section 3 includes the results and discussion over the findings and the evaluation process. Finally, in Section 4 we drew some conclusions and discuss on future directions.

2. Materials and methods

2.1. Generate CGH for engraving in fiber laser

Laser engraving over silver microstructures were accomplished with a Fiber laser of SISMA SpA on 1070 nm wavelength. All the reconstructed images were obtained using a HeNe laser that emits in 633 nm. The laser software needs to import the holographic masks belonging to specific input images. These masks were extracted from the, commercially available by LightTrans, VirtualLabFusion software [26] given the laser parameters and the appropriate pixel-size for this structure, which is 15 μm for this case.

For the design of the CGH by the specific software, Iterative Fourier Transform Algorithm (IFTA) optimization is commonly used, following an automated computational process [27–29]. However, for the same target image, the IFTA algorithm can produce numerous different CGHs providing that they meet the criteria set by the relevant cost functions. Although these CGHs produce the same target image upon illumination, they are certainly not all fabrication friendly. Tests showed that certain masks were engraved with the exact same laser parameters (pulse wavelength, power, number of passes) had non-feasible behaviour on silver. Indeed, experiments over different holographic masks of the same target image showed that a CGH with closely packed black pixels

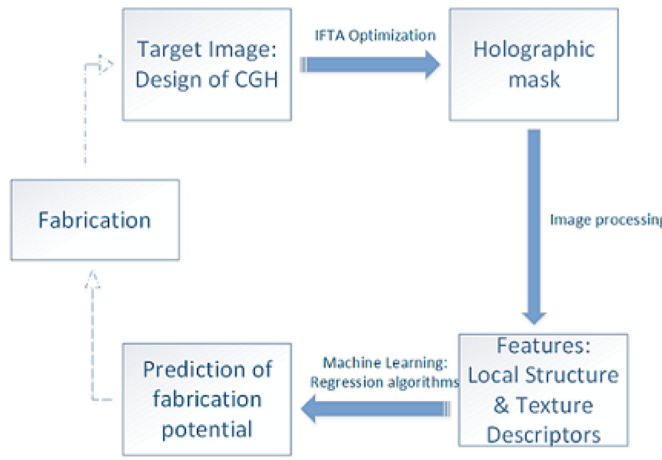

Fig. 1. The quality prediction scheme.

or with a very dense pattern, in terms of fabrication, translates to closely packed laser spots. In metals this leads to heating of the surface, with consequent change in the optical properties (absorption and reflection). To tackle this problem, the main consideration was to find an efficient way in order to distinguish holographic masks that would be difficult to etch on silver from those that would produce a successful engraving. Creating a "function" able to provide an estimation score for feasibility could definitely simplify the overall procedure and also maintain a good level of fabrication quality, minimizing both time and effort. The proposed method couples image analysis with pattern recognition techniques for the characterization of CGH masks designed using VirtualLab Fusion (Fig. 1). Digital images extracted from the software, that represent holographic masks, were used as input to the algorithm. For the next step, multiple and diverse features were extracted after image processing and several machine learning algorithms were applied to predict a score of feasibility of fabrication. The prediction model was constructed using as ground truth the evaluation scores of an expert rater that has performed numerous engravings of these structures on silver. Holographic masks with dense and large areas of black pixels are very difficult to fabricate. As discussed above, this is attributed to laser-surface heating and subsequent change in the reflection properties of the surface. Then score '1' was assigned to holographic masks of sparse dots, that can be fabricated easily, whereas '5' to holographic masks of dense black dot areas. Scores '2' to '4' were used to characterize the intermediate quality levels ('1' for very good, '2' for good, '3' for medium quality, '4', for bad and '5' for very bad quality). Methods for extraction and learning are described in detail in the following sections.

2.2. Dataset

Five different binary images of capital letters A, K, M, S, T were given as input to VirtualLab in order to produce holographic masks (Figs. 2,3). For each of those images, 40 different masks were created by changing the range of the default repetitions of the tool's optimization algorithms. The decision regarding the selection of these specific letters

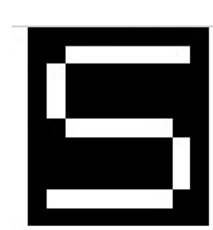

Fig. 2. Example of target image given as input to the software (capital letter S).

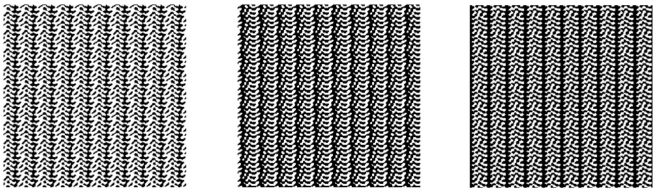

Fig. 3. Holographic masks for target image of letter S- figures: good quality (left) - medium rate (middle) - non-feasible result (right).

was based on their form, in order to pick a dataset with high diversity on forms and shapes for the algorithm. We used letters for which we verified the feasibility score of the corresponding holographic masks by constructing a few laser engravings per letter.

The total number of 200 images were annotated with their estimation score, according to the expert's experience from previous experimental work, and then we continued with feature extraction procedure.

2.3. Feature extraction and machine learning

Feature extraction is the procedure of extracting a set of characteristic variables that describe the data in a distinctive and representative way. In this case, we were searching for those features that are capable of identifying the differences between images that can be easily engraved on silver ("good" images) and images that cannot lead to a satisfying engraving ("bad" images). The technique revealed useful information about the holographic images and created the training dataset for the algorithm, to build a model. In the current study, the extracted features that were based on connecting component analysis are the following:

- Number of black objects (connected components) per image
- Number of white objects (connected components) per image
- Number of black pixel "neighborhoods" per image. The definition of black-pixel neighborhood refers to a 3 × 3 pixel block that have from 7 to 0 black pixels

In addition, we used morphological operators (non-linear filtering) in order to create well-defined shapes from the multiple identified components [30]. Dilation and Erosion operations with a 3 × 3 filter (4-connectivity) were applied on the images and the same shape characteristics were extracted from both the original and the dilated and eroded images. We also added one extra feature, a counter for the number of dilation repetitions required for an image component to become blank.

The last category of features is textural descriptors based on multiscale Gabor filters [31]. The 2D Gabor filter function is given by the following equation, where the spatial coordinates are denoted as (x,y):

$$\psi(x,y) = \frac{f^2}{\pi\gamma\eta} e^{-\left(\frac{f^2}{\gamma^2}x'^2 + \frac{f^2}{\eta^2}y'^2\right)} e^{j2\pi f x'},$$
$$x' = x\cos\theta + y\sin\theta$$
$$y' = -x\sin\theta + y\cos\theta \tag{1}$$

In the spatial domain the Gabor filter is 2D Fourier basis function multiplied by an origin-centred Gaussian, where f is the central frequency of the filter, θ the rotation angle, γ the sharpness (bandwidth) along the Gaussian major axis, and η the sharpness along the minor axis (perpendicular to the wave). In the frequency domain, the function is a single real-valued Gaussian centred at f, where (u,v) the frequency variable pair (Eq. (2)):

$$\Psi(u,v) = e^{-\left(\frac{\pi^2}{f^2}(\gamma^2(u'-f)+\eta^2 v'^2)\right)},$$
$$u' = u\cos\theta + v\sin\theta$$
$$v' = ux\sin\theta + v\cos\theta \tag{2}$$

Gabor features or Gabor bank are constructed from responses of Gabor filters in the above equations, by using multiple filters on several frequencies f_m and orientations θ_n [32]. Scalar metrics that were calculated from every image are the Gabor Square Energy and the Gabor Mean Amplitude. To recapitulate, the number of features computed for this training is: 10 features extracted from the connected component analysis (i.e., the number of black objects, the number of white objects and number of neighborhoods with 7 or 8 or 9 black pixels, one after dilation and one after dilation and erosion), 1 counter for the number of dilation repetitions required for an image component to become blank, and 80 features from the Gabor filters, i.e. 2 for every vector of the Gabor filter bank (Gabor Square Energy and Gabor Mean Amplitude). Therefore, the total number of features are 91.

The next step of this procedure is the construction of a prediction model to assess the extracted features of the holographic masks with their fabrication feasibility score. This is a problem that requires supervised machine learning, as we need a specific prediction based to a previous "labelling". Instead of using a classification method to build a 5-class prediction model, we chose to perform regression analysis that produces a continuous score. Regression analysis is a form of predictive modeling technique which examines the relationship between two or more variables of interest, dependent (target) and independent variables (predictor). There are various regression techniques that can be categorized related to the number of independent variables, the type of dependent variables and the shape of regression line. Each one of these techniques has its own equation and regression coefficients.

Some of the basic regression algorithms that had shown superior performance in various domains were selected for the construction of the current regression model. In order to train the model, we performed Support Vector Regression with different kernels (linear, gaussian, polynomial) and Regression trees. The optimal prediction over this precise dataset obtained from Support Vector Regression method, known as SVR, used with Gaussian Kernel. Support vector regression that was first presented from Vapnik [33] is widely used for prediction of nonlinear data, keeping the same concept that SVM follows for classification, i.e., create a linear function in a transformed feature space through kernel mapping [34]. In regression mode, the outcome is a real number. A margin of tolerance (ε) is set in approximation to the SVM. The target is to minimize the error within a certain threshold by tuning the hyperparameters that maximize the margin. The success of the transformation depends on the choice of the kernel function and its hyperparameters. The kernel functions transform the data into a higher dimensional feature space to enhance performance of linear separation.

$$y = \sum_{i=1}^{N} (a_i - a_i^*)\cdot\langle\varphi(x_i), \varphi(x)\rangle + b \tag{3}$$

where

$$\langle\varphi(x_i), \varphi(x)\rangle = K(x_i, x) \tag{4}$$

As φ we denote the mapping function that is used in order to make the non-linear version of the algorithm by mapping the data into a higher dimensional feature space. The algorithm depends on dot products between patterns x_i, so it suffices to know $K(x_i,x)$ instead of computing φ explicitly. The non-negative multipliers a_i and a_i^* for each observation x_i are used to construct the Lagrange dual function which solves the optimization problem in a computationally simple way. The variable b represents constant coefficient, which is used as an intercept.

Gaussian Kernel was in our case the kernel that results to most accurate prediction of the holographic mask's quality score (Eq. (5)).

$$k(x_i, x_j) = exp\left(-\frac{\|x_i - x_j\|^2}{2\sigma^2}\right) \quad (5)$$

where the adjustable parameter σ is important for the performance of the kernel and it must, therefore, be carefully adjusted to the problem.

To evaluate the regression prediction, we used the “Leave-one-out” method for cross-validation. The training dataset contained 90% of the dataset, and the test set was the remaining 10%. This process was repeated for 10 more times, leaving out each time a different 10% part of the total amount of data. At the end, the performance of all training repetitions was taken into consideration. The evaluation metric for the performance is Mean Absolute Error (MAE) in Eq. (6), which represents the mean of the absolute values of every initial quality score subtracted by its predicted quality score.

$$MAE = \frac{\sum_{i=1}^{n} abs(y_i - \lambda(x_i))}{n} \quad (6)$$

where y_i represents the prediction, x_i the true value and n the number of the observations.

The reason we chose MAE instead of MSE, which is more common for the evaluation of regression problems, is that MAE gives a more intuitive metric on the range of the predictions for every score level indicating the feasibility of production. Image processing analysis, feature extraction and regression modeling were implemented in MATLAB version R2018b [35].

3. Results and discussion

Fig. 4 shows the results from the Support Vector Regression method performed, after cross-validation. The bar diagram shows the percentage of instances of the test set that have error less than 0.5, between 0.5 and 1 and more than 1, in related to their pre-annotated score that has been declared on the initialization of the procedure. Fig. 5 shows the average error that has been calculated per score for the same test set. The MAE calculated for the Eq. (5) was 0.91, while with MAE for SVR linear kernel, SVR polynomial kernel and Regression trees was 2.64, 2.11 and 1.26 respectively.

It is observed that the categories of scores ‘2’, ‘3’ and ‘4’ have more samples with estimation error below 0.5 on this test set while instances with score ‘3’ seem to have the smallest error overall. In Fig. 5, we observe that the average prediction error is low for score ‘3’, but high enough for scores ‘1’ and ‘5’. This outcome can be attributed to the fact

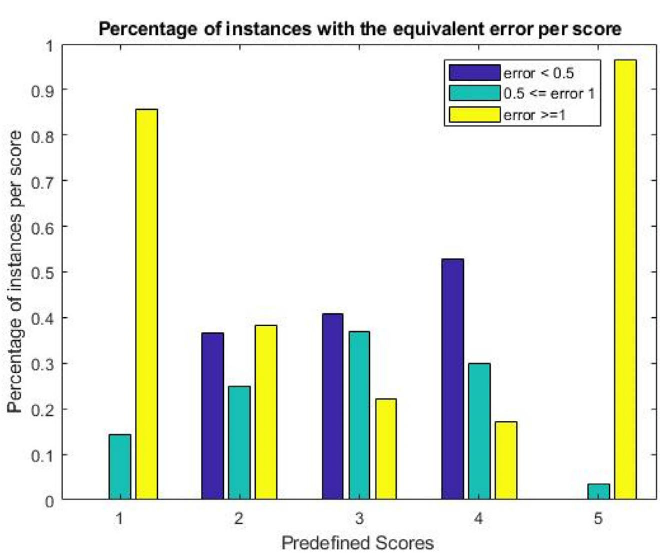

Fig. 4. Results from Support Vector Regression after cross-validation, Error for every different score of the test set (1: mask with highest quality potential of engraving, 5: mask with very low quality engraving).

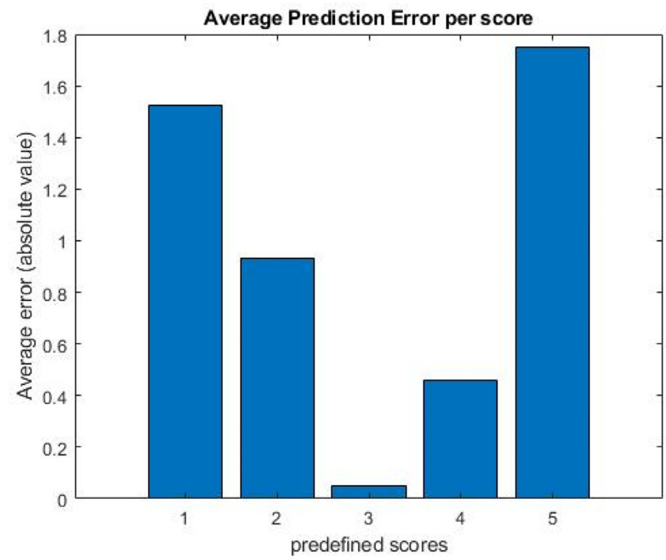

Fig. 5. Average Estimation Error per score.

that the score ‘3’ is the value that maximizes the likelihood in the least-squares sense, while values on the boundary of the distribution are much less likely. However, there is a significant distinction between the scores, especially between prediction score ‘1’ and scores ‘4’ and ‘5’. The average errors are almost non-overlapping, which indicates there exist a threshold between these categories for the distinction of engravings from feasible to difficult to be engraved.

Holographic mask patterns for letter ‘S' on silver were fabricated using a 1070 nm fiber laser (Figs. 6a and 7a). The two masks were characterized following the above procedure. Fig. 6 illustrates a mask with a high-quality reconstruction ranked with score ‘1’, in contrary to the mask in Fig. 7 which presents engraving and reconstruction of a low-quality mask with score ‘5’.

Both holograms were located on the same silver sample in close distance, and in both cases the engraving laser parameters were identical (power, pulse, frequency and the number of passes). The reconstruction of the image S for the CGH using a HeNe laser ($\lambda = 633nm$), depicted in Figs. 6a and 7a, is shown in Figs. 6b and 7b, respectively. These figures show the difference between the reconstructed images obtained from each CGH.

Regarding the machine learning prediction, a MAE of 0.91 indicates that the algorithm produces a very close number to the annotated estimation quality. This fact reassures that there is no possibility that a very good image with a score ‘1’ will have a prediction value close to ‘5’, and vice versa. Thus, if a user defines a threshold up to score ‘2’ to accept a CGH mask, that would allow him to obtain an image with very high potential of feasibility in terms of fabrication.

To the best of our knowledge, this is the first work aiming at the optimization of CGHs for fabrication on silver. Previous studies that have explored image processing and machine learning techniques, focus on general micromachining [36,37] in contrast to the present contribution, where we specify the procedures for manufacturable CGHs. In our case, deep learning was not an option as in [36], due to the limited amount of data that could be evaluated through experimental work with actual engravings.

4. Conclusions

We developed a novel approach for the engraving of CGH on silver using industrial fiber lasers. To this end, we employed machine learning algorithms and sophisticated image-based descriptors to develop a method for the distinction of CGHs in terms of manufacturability. The evaluation procedure showed an approximately 0.91 mean absolute

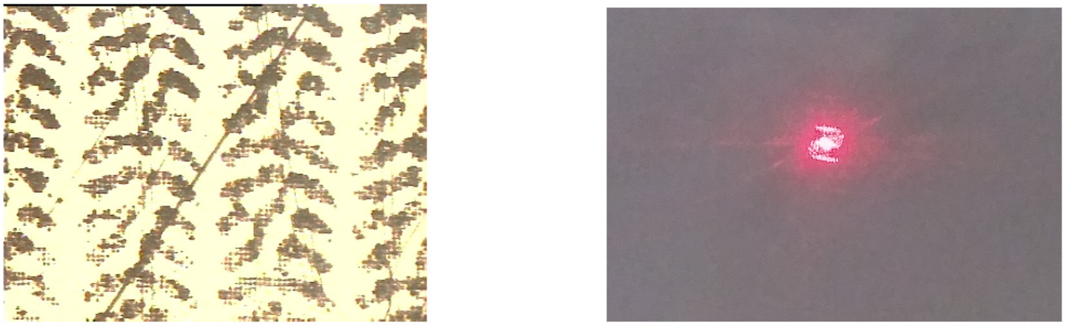

(a) Hologram of letter S engraved with a "good" mask (score '1').

(b) The reconstructed image of the hologram with the high-quality mask

Fig. 6. Hologram for letter 'S' engraved on silver with a fabricationally high-quality mask with score '1' and its reconstruction.

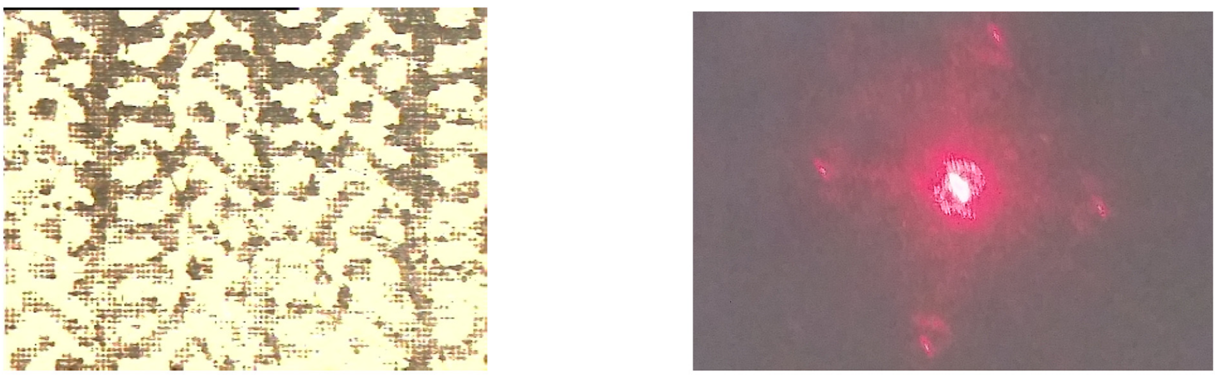

(a) Hologram engraved from a "bad" mask (score '5').

(b) Reconstructed image from the previous low-quality mask.

Fig. 7. Hologram for letter 'S' engraved on silver with a fabricationally low-quality mask with score '5' and its reconstruction.

error, which is a very promising result for an extended study over a much larger dataset. Our optimization technique could be a useful embedded function to any software that designs CGHs. This method can be elaborated for the construction of microstructures for security applications on precious metals and objects.

Declaration of Competing Interest

None.

Acknowledgments

This work is supported by the project "HELLAS-CH" (MIS 5002735), Greece which is implemented under the Action "Reinforcement of the Research and Innovation Infrastructure", funded by the Operational Programme "Competitiveness, Entrepreneurship and Innovation" (NSRF 2014-2020) and co-financed by Greece and the European Union (European Regional Development Fund). Provision of the fiber laser source by SISMA S.p.A. is gratefully acknowledged.

References

[1] B. Kemper, L. Pohl, M. Kaiser, E. Döpker, J. Schnekenburger, S. Ketelhut, Label-Free Detection of Global Morphology Changes in Confluent Cell Layers Utilizing Quantitative Phase Imaging with Digital Holographic Microscopy, Clinical and Preclinical Optical Diagnostics II, EB101 SPIE Proceedings (Optical Society of America), 2019, p. 30 11076.
[2] V. Bianco, L. Miccio, P. Memmolo, F. Merola, B. Mandracchia, T. Cacace, M. Mugnano, M. Paturzo, M. Villone, P.L. Maffettone, P. Ferraro, 3D Imaging in Microfluidics: New Holographic Methods and Devices, Microfluidics, BioMEMS, and Medical Microsystems XVII, 10875 Proc. SPIE, 2019.
[3] M.R. Abuturab, Securing multiple information using wavelet transform and Yang-Gu mixture amplitude-phase retrieval algorithm, Opt. Lasers Eng. 118 (2019) 42–51.
[4] M.-L. Piao, Y.-L. Piao, N. Kim, 3D Image Encryption Based on Computer-Generated Hologram in the Fractional Fourier Domain, (2020), p. 37.
[5] C. Zhao, J.H. Burge, Optical testing with computer generated holograms: comprehensive error analysis, Opt. Manuf. Test. X 8838 (2013) 88380H.
[6] K. Wakunami, H. Yamashita, M. Yamaguchi, Occlusion culling for computer generated hologram based on ray-wavefront conversion, Opt. Express 21 (2013) 21811.
[7] K. Wakunami, M. Yamaguchi, Occlusion processing for computer generated hologram by conversion between the wavefront and light-ray information, J. Phys. Conf. Ser. 415 (2013).
[8] K.L. Wlodarczyk, M. Ardron, N.J. Weston, D.P. Hand, Holographic watermarks and steganographic markings for combating the counterfeiting practices of high-value metal products, J. Mater. Process. Technol. 264 (2019) 328–335.
[9] D. Abookasis, J. Rosen, Three types of computer-generated hologram synthesized from multiple angular viewpoints of a three-dimensional scene, Appl. Opt. 45 (2006) 6533–6538.
[10] R.H. Chen, T.D. Wilkinson, Computer generated hologram from point cloud using graphics processor, Appl. Opt. 48 (2009) 6841–6850.
[11] P.W. Tsang, T.C. Poon, K.W. Cheung, Fast numerical generation and encryption of computer-generated Fresnel holograms, Appl. Opt. 50 (2011).
[12] S. Hasegawa, Y. Hayasaki, Second-harmonic optimization of computer-generated hologram, Opt. Lett. 36 (2011) 2943.
[13] Y. Pan, Y. Wang, J. Liu, X. Li, J. Jia, Fast polygon-based method for calculating computer-generated holograms in three-dimensional display, Appl. Opt. 52 (2013).
[14] A.J. Antoczak, B. Stepak, P.E. Kozio, K.M. Abramski, The influence of process parameters on the laser-induced coloring of titanium, Appl. Phys. A 115 (2014) 1003–1013.
[15] V. Veiko, G. Odintsova, E. Ageev, Y. Karlagina, A. Loginov, A. Skuratova, E. Gorbunova, Controlled oxide films formation by nanosecond laser pulses for color marking, Opt. Express 22 (2014) 24342.
[16] T. Murphy, P. Harrison, S. Norman, Black anneal marking with pulsed fiber lasers, Ind. Laser Appl. Symp. 9657 (2015) (96570I).
[17] C. Martinez, O. Lemonnier, F. Laulagnet, A. Fargeix, F. Tissot, M.F. Armand, Complementary computer generated holography for aesthetic watermarking, Opt. Express 20 (2012) 5547.
[18] C. Martinez, F. Laulagnet, O. Lemonnier, Gray tone image watermarking with complementary computer generated holography, Opt. Express 21 (2013) 15438.
[19] G. Tricoles, Computer generated holograms: an historical review, Appl. Opt. 26

(1987) 4351.
[20] K.L. Wlodarczyk, J.J. Kaakkunen, P. Vahimaa, D.P. Hand, Efficient speckle-free laser marking using a spatial light modulator, Appl. Phys. A 116 (2014) 111–118.
[21] K.L. Wlodarczyk, M. Ardron, A.J. Waddie, A. Dunn, M.D. Kidd, N.J. Weston, D.P. Hand, Laser microsculpting for the generation of robust diffractive security markings on the surface of metals, J. Mater. Process. Technol. 222 (2015) 206–218.
[22] K.L. Wlodarczyk, N.J. Weston, M. Ardron, D.P. Hand, Direct CO_2 laser-based generation of holographic structures on the surface of glass, Opt. Express 24 (2016) 1447.
[23] K.L. Wlodarczyk, M. Ardron, A.J. Waddie, M.R. Taghizadeh, N.J. Weston, D.P. Hand, Tamper-proof markings for the identification and traceability of high-value metal goods, Opt. Express 25 (2017) 15216.
[24] SPI LASERS, Advantages and Benefits of Fiber Lasers, https://www.spilasers.com/industrial-fiber-lasers/advantages-and-benefits-of-fiber-lasers/.
[25] L. Justin Hanna, Five Top Advantages of Fiber Laser Cutting, http://www.preferredmachinellc.com/why-fiber-laser-cutting.
[26] LightTrans, VirtualLab Fusion, https://www.lighttrans.com.
[27] V.A. Soifer, Computer Design of Diffractive Optics, (2012).
[28] A. Vijayakumar, S. Bhattacharya, A. Vijayakumar, S. Bhattacharya, Design of diffractive optical elements, Design and Fabrication of Diffractive Optical Elements with MATLAB, 2017.
[29] D.Y. Alsaka, Ç. Arpali, S.A. Arpali, A comparison of iterative Fourier transform algorithms for image quality estimation, Opt. Rev. 25 (2018) 625–637.
[30] J.I. Liang, J. Piper, J.Y. Tang, Erosion and dilation of binary images by arbitrary structuring elements using interval coding, Pattern Recogn. Lett. 9 (1989) 201–209.
[31] J.K. Kamarainen, Gabor features in image analysis, 2012 3rd International Conference on Image Processing Theory, Tools and Applications, IPTA, 2012, pp. 13–14.
[32] M. Haghighat, S. Zonouz, M. Abdel-Mottaleb, CloudID: trustworthy cloud-based and cross-enterprise biometric identification, Expert Syst. Appl. 42 (2015) 7905–7916.
[33] V. Vapnik, Statistical Learning Theory, 1998 (1998).
[34] A.J. Smola, B. Schölkopf, A Tutorial on Support Vector Regression, (2004).
[35] Matlab, MATLAB: The Language of Technical Computing, http://www.mathworks.com/products/matlab/.
[36] B. Mills, D.J. Heath, J.A. Grant-Jacob, Y. Xie, R.W. Eason, Image-based monitoring of femtosecond laser machining via a neural network, J. Phys. 1 (2018) 015008.
[37] H. Tercan, T.A. Khawli, U. Eppelt, C. Büscher, T. Meisen, S. Jeschke, Use of classification techniques to design laser cutting processes, Procedia CIRP, 52 Elsevier B.V., 2016, pp. 292–297.